Design and Analysis of Landing Trajectories and Low-Altitude Asteroid Flyovers

D. J. Scheeres[1]

This article discusses the dynamics, analysis, and design of low-altitude flyovers and landing trajectories at asteroids. The theory presented in the article will be applicable to asteroid missions in general. The article will begin with a brief review of orbital dynamics in close proximity to asteroids or other irregularly shaped bodies, covering the special considerations that must be taken into account for this class of problem. Then, the specific types of trajectories to be considered will be introduced, along with the basic computations that must be performed to support and generate these trajectories. These trajectories will be limited to two classes, ones that have periapsis "close" to the central body—with close being defined as near or within the circumscribing sphere about the asteroid—and those that intersect with the asteroid surface. Such landing trajectories usually have several maneuvers during descent to the surface in order to minimize impact speeds. An analysis of a low-altitude flyover trajectory is made that includes analytical results that can be inferred from the dynamical theories, and Monte Carlo analyses that explore the non-linear dynamics over finite regions of phase space.

I. Introduction

Asteroid orbiter missions are now a demonstrated fact with the success of the Near Earth Asteroid Rendezvous (NEAR) Shoemaker mission. Future missions to asteroids will benefit greatly from the NEAR experience; thus, a detailed discussion of the actual and possible orbit options of NEAR at Eros is warranted. In [11] the orbit dynamic characterization of the Eros environment was given, with an emphasis on the natural dynamics that an orbiting spacecraft would experience. In this contribution, we review the relevant sections of that article and describe how orbital options that bring the spacecraft into close proximity to the asteroid surface can be understood and designed.

The peculiarities of spacecraft motion in the vicinity of an asteroid such as Eros are due mainly to the interaction of the spacecraft trajectory with the rotating second-degree and -order gravity field of the asteroid. For asteroids such as Eros, where the synchronous orbit radius lies relatively close to the asteroid, most orbits within $\sim$5 mean radii are unstable and are subject to impact or escape from the asteroid. Exceptions to these are orbits that are retrograde and close to the equatorial plane. These dynamics are reviewed in [11].

[1] Department of Aerospace Engineering, The University of Michigan, Ann Arbor.

The research described in this publication was carried out by the Jet Propulsion Laboratory, California Institute of Technology, under a contract with the National Aeronautics and Space Administration.

Of special interest for many future asteroid missions will be how to bring a spacecraft into close proximity to the surface of an asteroid without jeopardizing the spacecraft or mission [1]. For these applications, it is usually desired to reduce the relative speed between the spacecraft and the surface to acceptable levels, which generally rules out the use of equatorial, retrograde orbits. The two main classes of close-proximity orbit that this calls for can be characterized as low-altitude flyovers and landing trajectories. We do not consider hovering trajectories [10,5] as these generally require a level of navigation technology beyond that found in the NEAR spacecraft.

In both of the situations considered here, the spacecraft will descend from a stable orbit at a higher altitude along a nominally elliptic orbit down to a periapsis at a given altitude above the asteroid surface. A low-altitude flyover continues through its orbital motion and rises back to its new apoapsis radius (which can differ markedly from its initial radius). A landing trajectory would initiate additional maneuvers that would bring it down to a controlled descent and eventual impact on the surface (a variation would artificially terminate a landing trajectory early to boost the spacecraft back into orbit prior to surface touchdown). In both of these scenarios, the spacecraft is subject to strong gravity field perturbations as it descends—perturbations that can be understood in an approximate sense and used to design these trajectories.

II. Models

A. General Asteroid Model

The general model for a uniformly rotating asteroid consists of a rotation period and a gravity field. The standard gravity field model used for navigation operations about a small body is the spherical harmonic expansion field, which can be estimated from the radio metric data, combined with optical data to fix the relative orientation of the asteroid with respect to the spacecraft [4]. The usual specification of this field is truncated at some degree and order and is expressed as

$$U = \frac{\mu}{r} \sum_{i=0}^{N} \sum_{j=0}^{i} \left(\frac{R_o}{r} \right)^i P_i^j(\sin\delta) \left[C_{ij} \cos(j\lambda) + S_{ij} \sin(j\lambda) \right] \tag{1}$$

where μ is the asteroid mass times the universal gravitational constant; R_o is the normalizing radius, usually taken as either the radius of the circumscribing sphere about the asteroid or the mean volumetric radius; P_i^j is the associated Legendre function; C_{ij} and S_{ij} are the spherical harmonic gravity coefficients; and r, δ, and λ are the radius, latitude and longitude coordinates, respectively, of the spacecraft in the asteroid fixed frame. Usually, the gravity field is expanded about the center of mass of the asteroid, yielding $C_{1j} = S_{11} = 0$, and with its coordinate axes oriented so that they lie along the principal axes of inertia, yielding $C_{21} = S_{21} = S_{22} = 0$.

The spherical harmonic gravity field is the best descriptor of the asteroid gravity field when outside of the circumscribing sphere about the asteroid (the circumscribing sphere is the sphere of minimum radius that contains the asteroid, centered at the expansion center of the gravity field). When inside of this sphere, the spherical harmonic expansion field may diverge and no longer yield accurate information about the true gravity field. For most orbital applications, this divergence is not of great concern, as the spacecraft will normally remain outside of this circumscribing sphere. For situations in which a landing or extremely close pass over the asteroid surface is desired, however, this divergence will affect the design, prediction, and control of the spacecraft orbit. In these situations, it is necessary to specify the asteroid gravity field using a formulation that does not diverge. There are several different approaches to this problem; the one that we use here is based on modeling the gravity field of the asteroid as the summation of gravity fields of tetrahedra, for which a closed-form formula is known [14,15]. All numerical integrations proposed or shown herein will use the tetrahedron formulation whenever within the circumscribing radius of the asteroid.

B. Equations of Motion

There are two forms of the equations of motion that are useful for our analysis. The first states the equations in the body-fixed frame, hence a frame with uniform rotation. In this coordinate system, the central gravity field does not change with time, and since the rotational rate of the asteroid does not change either, the equations of motion are time invariant.

In the body-fixed reference frame, the equations of motion are

$$\ddot{x} - 2\omega_E \dot{y} = \omega_E^2 x + U_x \tag{2}$$

$$\ddot{y} + 2\omega_E \dot{x} = \omega_E^2 y + U_y \tag{3}$$

$$\ddot{z} = U_z \tag{4}$$

where x, y, and z are measured along the asteroid's minimum, intermediate, and maximum moment of inertia axes in the body-fixed frame, ω_E is the rotation rate of the asteroid, and U represents the gravitational potential of the asteroid. Since these equations are time-invariant, an additional integral of motion exists (termed the Jacobi constant) and is

$$J = \frac{1}{2}\left(\dot{x}^2 + \dot{y}^2 + \dot{z}^2\right) - \frac{1}{2}\omega_E^2\left(x^2 + y^2\right) - U \tag{5}$$

For our analytical computations, it is more useful to use the "canonical" form of the Lagrange planetary equations [2], which express the change in orbit Keplerian energy, angular momentum, and angular momentum projected onto the z-axis as a function of the gravitational perturbations acting on them. The equations describing the change of these variables can then be expressed as

$$\frac{dC}{dt} = \frac{\partial R}{\partial t} \tag{6}$$

$$\frac{dG}{dt} = \frac{\partial R}{\partial \omega} \tag{7}$$

$$\frac{dH}{dt} = \frac{\partial R}{\partial \Omega} \tag{8}$$

where

$$C = \frac{-\mu}{2a} \tag{9}$$

$$G = \sqrt{\mu a(1 - e^2)} \tag{10}$$

$$H = G\cos i \tag{11}$$

$$R = U - \frac{\mu}{r} \tag{12}$$

and a, e, i, ω, and Ω are the osculating orbital elements. Equations (7) and (8) are taken from classical results [2] while Eq. (6) is derived by applying the chain rule, taking the partial of R with respect to the true anomaly f first and then taking the partial of the true anomaly f with respect to the time [8]. Note that we neglect to add the additional equations describing the dynamics of the argument of periapsis, longitude of the ascending node, and mean epoch, as we will not explicitly study those equations here. The Jacobi integral can be restated in terms of these basic variables:

$$J = C - \omega_E H - R \tag{13}$$

The strongest perturbation that the trajectory feels when in close proximity to the asteroid is mainly due to the second-degree and -order gravity field of the rotating body [11], which has the explicit form

$$U_{20+22} = \frac{\mu R_o^2}{r^3}\left[C_{20}\left(1 - \frac{3}{2}\cos^2\delta\right) + 3C_{22}\cos^2\delta\,\cos 2\lambda\right] \tag{14}$$

For our analytical estimates, we will only consider the contribution from these terms.

III. Dynamics of Close Trajectories

Although the orbital dynamics are best computed using numerical integrations, a class of estimates for the change in orbit energy and angular momentum can be derived that provides a great deal of insight into the effect of a close flyby on the resulting orbit. The basic application of this theory is found in [9], and the results are restated here. Of particular interest are the change in orbit parameters as a spacecraft descends from a relatively high apoapsis to a periapsis close to the asteroid surface and the change in orbit parameters as the spacecraft travels through a full orbit, from apoapsis to apoapsis. In the following, we state explicit formulae for the change in energy, C; angular momentum, G; and the projection of the angular momentum along the z axis, H. Changes in these parameters can be related to changes in the classical orbital elements [13].

A. Half-Orbit Perturbations

Over an orbit transfer from apoapsis to periapsis, we find variations in the orbital elements due to both the C_{20} and the C_{22} gravity coefficients.

The projected angular momentum, H, is identically conserved under perturbation from C_{20}, and thus will not vary. The energy and total angular momentum, C and G, will vary over a half orbit, however, yielding changes of

$$\Delta G_{C_{20}} = 2\sqrt{\frac{\mu}{p^3}}C_{20}\cos 2\omega \sin^2 ie \tag{15}$$

$$\Delta C_{C_{20}} = \frac{\mu}{2p^3}C_{20}\Big[-1 + 3\left(\cos^2 i + \sin^2 i\cos 2\omega\right)\Big]\left(3 + e^2\right)e \tag{16}$$

Similarly, and leading to more detailed results, the change in orbit elements C, G, and H due to C_{22} over one-half of an orbit can also be predicted approximately:

$$\Delta G_{C_{22}} = -3C_{22}\sqrt{\frac{\mu}{p^3}}\left[\cos^4\left(\frac{i}{2}\right)\left\{\sin 2(\omega+\Omega)I_2^1 + \cos 2(\omega+\Omega)J_2^1\right\}\right.$$

$$\left. + \sin^4\left(\frac{i}{2}\right)\left\{\sin 2(\omega-\Omega)I_{-2}^1 - \cos 2(\omega-\Omega)J_{-2}^1\right\}\right] \tag{17}$$

$$\Delta H_{C_{22}} = -3C_{22}\sqrt{\frac{\mu}{p^3}}\left[\frac{1}{2}\sin^2 i\left\{\sin 2\Omega I_0^1 + \cos 2\Omega J_0^1\right\}\right.$$

$$+ \cos^4\left(\frac{i}{2}\right)\left\{\sin 2(\omega+\Omega)I_2^1 + \cos 2(\omega+\Omega)J_2^1\right\}$$

$$\left. - \sin^4\left(\frac{i}{2}\right)\left\{\sin 2(\omega-\Omega)I_{-2}^1 - \cos 2(\omega-\Omega)J_{-2}^1\right\}\right] \tag{18}$$

and the variation in C can be found from the Jacobi integral. The integrals I_m^n and J_m^n have the definitions

$$I_m^n = 2\int_0^\pi (1+e\cos f)^n \cos(mf - 2\omega_E t)\, df \tag{19}$$

$$J_m^n = 2\int_0^\pi (1+e\cos f)^n \sin(mf - 2\omega_E t)\, df \tag{20}$$

These integrals cannot be expressed in closed form in general except for the particular cases

$$I_0^{-2} = \frac{\sin\left(2\pi\sqrt{\omega_E^2 a^3/\mu}\right)}{\sqrt{\omega_E^2 p^3/\mu}} \tag{21}$$

$$J_0^{-2} = \frac{\cos\left(2\pi\sqrt{\omega_E^2 a^3/\mu}\right)}{\sqrt{\omega_E^2 p^3/\mu}} \tag{22}$$

The numerical quadrature of these integrals has been treated previously [9]. We note that these integrals are intimately related to the Hansen coefficients [12]. Figures 1 and 2 show the values of these integrals over an interval of parameter values of interest. The total variation in these elements over an apoapsis-to-periapsis passage is then computed as

$$\Delta G = \Delta G_{C_{20}} + \Delta G_{C_{22}} \tag{23}$$

$$\Delta H = \Delta H_{C_{20}} + \Delta H_{C_{22}} \tag{24}$$

$$\Delta C = \Delta C_{C_{20}} + \Delta C_{C_{22}} \tag{25}$$

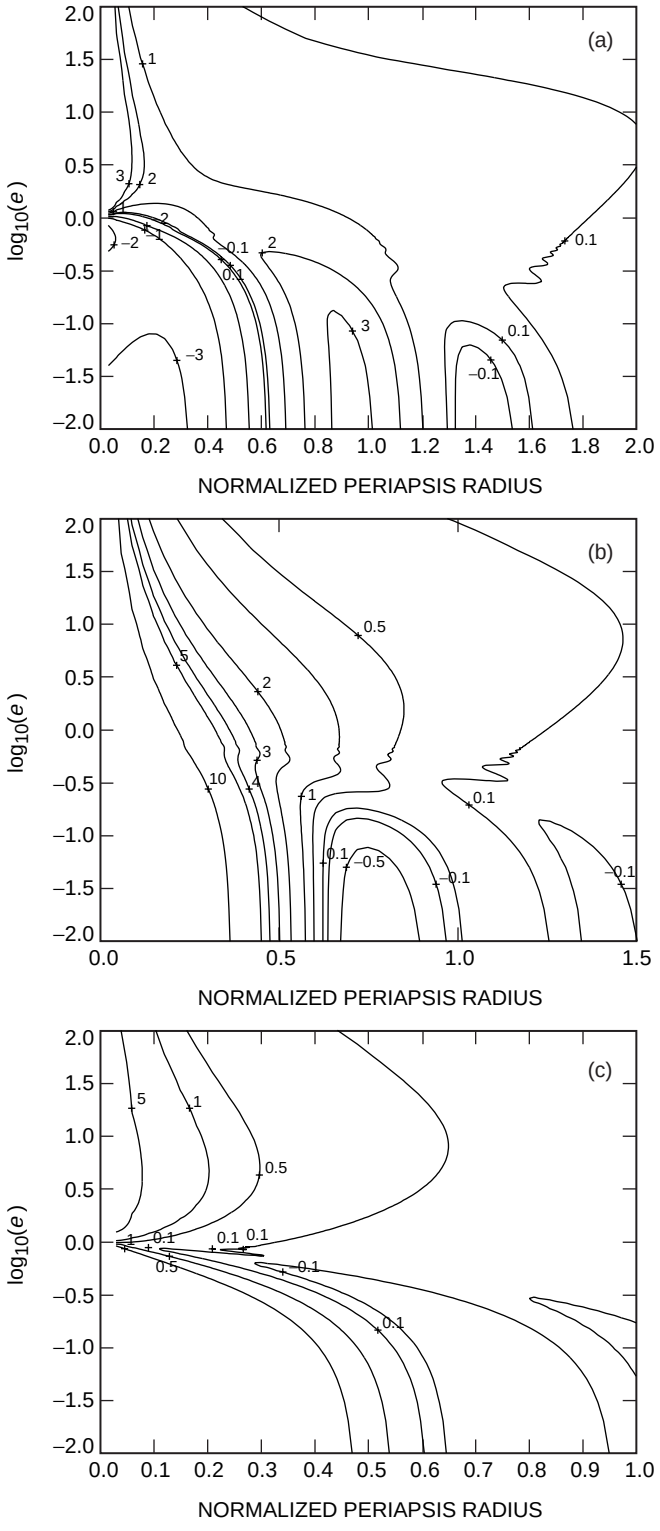

Fig. 1. Contour plots of integrals (a) I^1_2 / $(2p^{3/2})$, (b) I^1_0 / $(2p^{3/2})$, and (c) I^1_{-2} / $(2p^{3/2})$. The normalized periapsis radius is defined as $q\,(\omega_E^2/\mu)^{1/3}$, where q is the dimensional periapsis radius.

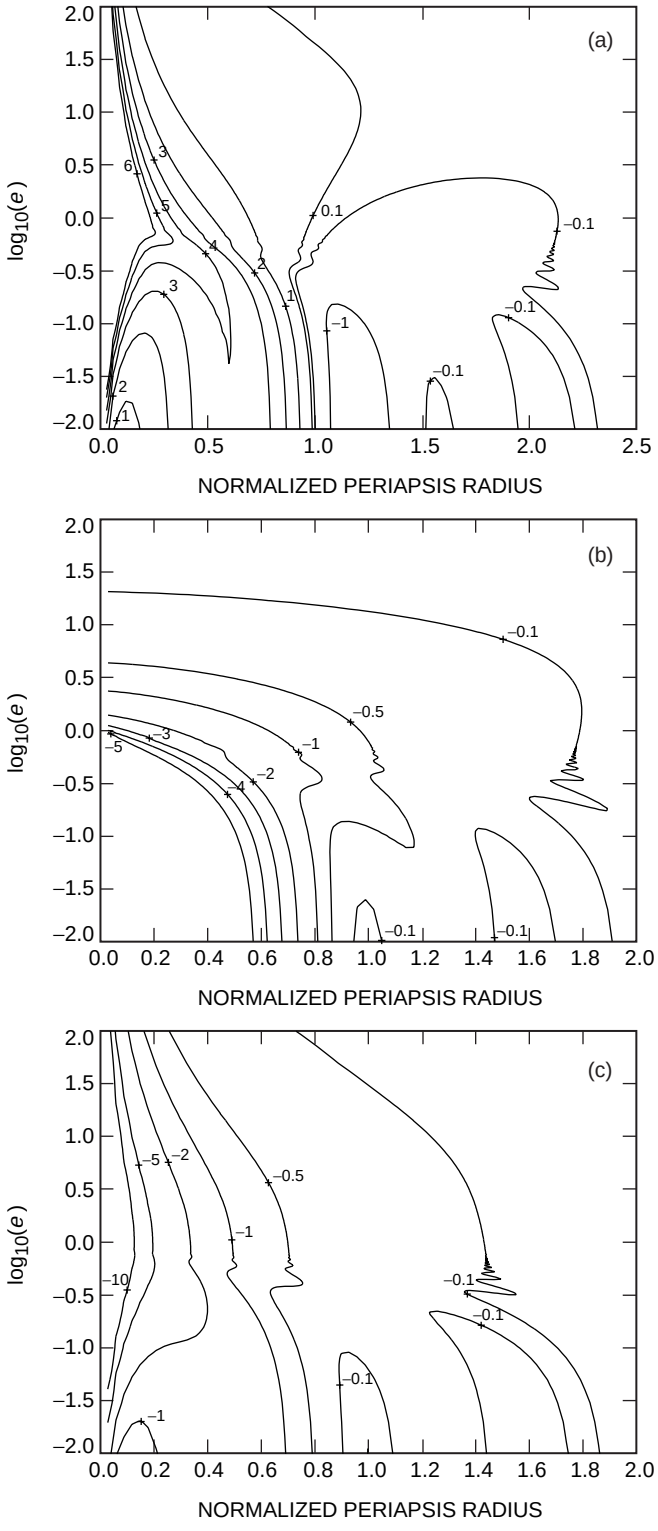

Fig. 2. Contour plots of integrals (a) $J^1_2 / (2p^{3/2})$, (b) $J^1_0 / (2p^{3/2})$, and (c) $J^1_{-2} / (2p^{3/2})$. The normalized periapsis radius is defined as $q\,(\omega_E^2/\mu)^{1/3}$, where q is the dimensional periapsis radius.

Using these results, it is possible to predict the change in orbital parameters between apoapsis of the transfer ellipse to periapsis of the ellipse. In general, the variation in energy and angular momentum can be quite large, implying that using Keplerian orbits to initiate numerical targeting routines may be an inefficient way in which to choose a target flyover condition. Rather, using the above relations in the initial design of a de-orbit maneuver can provide additional insight into the selection of target points on the asteroid surface.

B. Full-Orbit Perturbations

For analysis of the low-altitude flyovers, the orbit is continued through periapsis up to its next apoapsis passage, experiencing additional perturbations along the way. For the effect of the C_{20} gravity term, these additional perturbations erase the fluctuations in angular momentum and energy. For the C_{22} effects, however, only a partial cancellation occurs, leaving a residual change in the orbit elements that is often rather large [9,11]. The results are similar to the half-orbit results, except that the integrals J_m^n will cancel out over a full-orbit pass, leaving only the terms containing the integrals I_m^n:

$$\Delta G = -6C_{22}\sqrt{\frac{\mu}{p^3}}\left[\cos^4\frac{i}{2}\sin 2(\omega+\Omega)I_2^1 + \sin^4\frac{i}{2}\sin 2(\omega-\Omega)I_{-2}^1\right] \tag{26}$$

$$\Delta H = -6C_{22}\sqrt{\frac{\mu}{p^3}}\left[\frac{1}{2}\sin^2 i\sin 2\Omega I_0^1 + \cos^4\frac{i}{2}\sin 2(\omega+\Omega)I_2^1 - \sin^4\frac{i}{2}\sin 2(\omega-\Omega)I_{-2}^1\right] \tag{27}$$

$$\begin{aligned}\Delta C = &-6C_{22}\omega_E\sqrt{\frac{\mu}{p^3}}\left[\frac{1}{2}\sin^2 i\sin 2\Omega\left\{I_0^1-(1-e)^3I_0^{-2}\right\}\right.\\ &\left.+\cos^4\frac{i}{2}\sin 2(\omega+\Omega)\left\{I_2^1-(1-e)^3I_0^{-2}\right\}-\sin^4\frac{i}{2}\sin 2(\omega-\Omega)\left\{I_{-2}^1-(1-e)^3I_0^{-2}\right\}\right]\end{aligned} \tag{28}$$

Note from Fig. 1 that $I_2^1 \gg I_{-2}^1$ and $I_2^1 \gg I_0^1$ in the regions that interest us. Thus, direct, low-inclination orbits will be subject to the terms I_2^1 while retrograde, near-equatorial orbits will be primarily subject to the terms I_{-2}^1. Inspecting the contour plots, it is obvious that direct orbits will experience much larger changes in energy and angular momentum for each orbit, while the retrograde orbits will experience little, if any, change per orbit. This result explicitly predicts the relative stability of retrograde orbits noticed previously in the literature [3,6–8] and predicts the large variations in energy and angular momentum in a concise and clear fashion. In the design discussion, we will neglect I_{-2}^1 and I_0^1 to gain a simpler form for Eqs. (26) through (28).

C. Landing Dynamics

For a surface landing, the spacecraft must initiate a series of additional maneuvers once it arrives in the vicinity of periapsis of its transfer orbit from a higher altitude. To "land" on the asteroid surface requires only that the periapsis of the spacecraft orbit be placed below the asteroid surface.

The half-orbit results stated earlier describe how the transfer orbit's energy and angular momentum vary as the spacecraft transitions to the periapsis of its initial orbit. At the time of closest approach, the spacecraft must perform a maneuver to transition into an impacting orbit. When close to the asteroid, it is not desirable to spend long periods of time moving under the attraction of the rotating body. Thus, a transfer to a subsequent elliptic orbit with apoapsis at the transfer orbit periapsis and the new periapsis at some lower, but still positive, altitude above the asteroid is ill-advised as such a transfer would take hours, in general, and would entail subjecting the trajectory to strong perturbations that would change the target periapsis conditions and, thus, would have to be modeled in detail. Due to the strong perturbations

from the gravity field, a trajectory in such close proximity is highly unstable, and small initial errors in the state of the spacecraft and in the orbit maneuvers would cause the resulting uncertainty distribution of the spacecraft to be spread out over a wide region of phase space.

Thus, the natural solution is to place the spacecraft on a nearly rectilinear orbit, so that the periapsis will be well below the surface and the trajectory of the spacecraft in inertial space will approximate a straight line. With such a model, an approximate relation between maneuver altitude and impact speed can be found from the Keplerian energy equation (which does not strictly hold, but can still be used to obtain reasonable estimates of impact speed):

$$V_{imp} = \sqrt{\frac{2\mu h}{R(R+h)}} \tag{29}$$

Due to the non-spherical mass distribution of the asteroid, this relationship can be quite inaccurate at certain regions of the body. If we define the gravitational potential of the asteroid at its surface as $U(\mathbf{R})$, for which we cannot use the classical spherical harmonic expansion due to divergence problems near the surface, then a better approximation is

$$V_{imp} = \sqrt{\frac{2h}{R+h}U(\mathbf{R})} \tag{30}$$

For an assumed $\mu \sim 4.46 \times 10^{-4}$ km^3/s^2 and $R \sim 9$ km, we can find the maximum altitude of a braking maneuver in order to achieve a given impact speed on the surface, as shown in Fig. 3.

The above result is ideal in more than one way, however, in that it also does not factor in the rotation of the asteroid surface. Due to the rotation of the asteroid, any particular location on the surface of Eros, $\mathbf{R}_o$, has an inertial velocity of

$$\mathbf{V}_o = \omega_E \hat{\mathbf{z}} \times \mathbf{R}_o \tag{31}$$

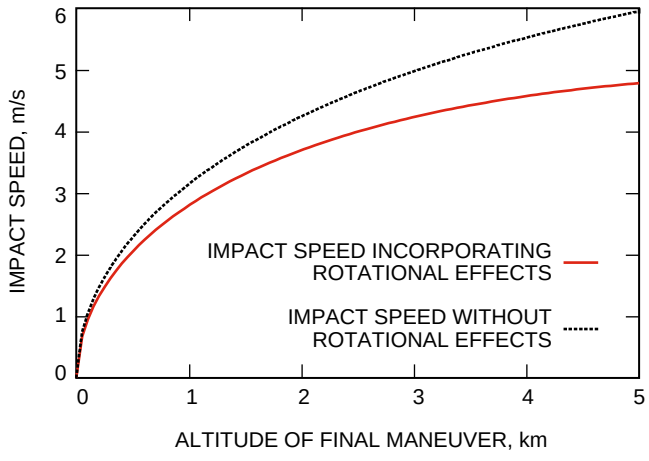

Fig. 3. The maximum altitude of the final maneuver versus the inertial impact speed at Eros, derived assuming a point mass Eros. The effect of asteroid rotation is shown.

where ω_E is the rotation rate of Eros. Thus, if a spacecraft has an inertial velocity vector $\mathbf{v}$ at impact, the body relative speed will be

$$\mathbf{v}_{rel} = \mathbf{v} - \mathbf{V}_o \tag{32}$$

On Eros, the inertial surface speeds range from 0 at the poles up to almost 6 m/s at the ends of the asteroid. Thus, it is possible to achieve impact speeds lower than a simple computation would indicate by the proper placement of the final de-orbit maneuvers. A simple consideration of the relative dynamics indicates that a landing site chosen on the "trailing edge" of an asteroid—that is, a point on the surface where the inertial speed of the asteroid is directed in the opposite direction to the surface normal—will result in the minimum impact speed, or minimum relative speed, for a given transfer orbit. However, a typical surface speed on Eros would be on the order of 3.3 m/s, which compares to a local circular speed of 6.7 m/s. A direct transfer ellipse would have periapsis speeds greater than this, in general indicating that a relative speed greater than 3 m/s is the best one could hope for using a direct transfer from a higher orbit to an impact site on the trailing edge of the asteroid.

Thus, to fully utilize the rotation of the asteroid to minimize impact speed will still require a maneuver close to the surface. Taking into account the trajectory relative to the asteroid surface, we find the acceleration of a spacecraft to be modified somewhat. In an ideal case (assuming point mass gravity), the relevant equations for motion close to the surface include the effect of centripetal and Coriolis accelerations, which can reduce the impact speed, leading to an ideal estimate:

$$V_{imp} = \sqrt{\frac{2\mu h}{R(R+h)} - \omega_E^2(2R+h)h} \tag{33}$$

which is derived from the Jacobi constant, Eq. (5). The resulting impact curve incorporating rotation effects is shown in Fig. 3 and yields some decrease in predicted impact speed.

With or without rotational effects taken into consideration, the final trajectory of a landing spacecraft can be modeled approximately as a descent in a constant acceleration field relative to the surface, the constant acceleration arising from a combination of gravitational attraction and rotational accelerations due to the rotating frame. Thus, control of impact speed reduces to control of rate of altitude descent. This is a problem ideally suited to a limited autonomy, where an altimeter senses the rate of descent and altitude and a simple control algorithm computes and enacts the necessary thrust to reduce the predicted impact speed. In the absence of such an autonomous navigation capability, the de-orbit maneuvers must be planned in advance and performed in an open-loop fashion, which can result in relatively large dispersions in impact time, speed, and location.

In this situation, there will be a trade-off between the number of maneuvers performed and the likelihood of achieving a given impact speed and site. Ideally, one braking maneuver would be planned near the asteroid surface, thus yielding a minimal impact speed. However, the altitude of such a maneuver will be low, and due to uncertainties in the spacecraft trajectory and asteroid model, there is a significant chance that impact may occur prior to the maneuver, yielding a high probability of a large impact speed. As the initial braking maneuver is moved to higher altitudes, the probability of being able to perform the maneuver increases. Thus, performing a maneuver at a higher altitude can ensure that the impact speed is at least limited to a given value, albeit larger than may be desired. Then, however, it is possible to add an additional maneuver at a lower altitude and again perform an open-loop braking maneuver to decrease the impact speed. Again, the probability of this maneuver occurring is reduced, due to the initial state and model uncertainties and the added uncertainties from the initial braking maneuver. Still, the overall impact of missing this maneuver has been reduced by the placement of the initial, higher

maneuver. This chain of reasoning can be repeated, leading to multiple braking maneuvers during the descent phase. This is not a fuel-optimal descent strategy, which would delay the initial maneuver until as late as possible, but this is not an issue due to the relatively low values of ΔV maneuvers needed (on the order of meters/second).

IV. Design

A. Low-Altitude Flyover Design

In the design of low-altitude flyovers, the main navigation safety issue is to ensure that the next periapsis passage is far enough away that the spacecraft will not risk going through periapsis again—or in other words, to make sure that control of the spacecraft can be recovered and a maneuver to place the spacecraft into a "safe" orbit is performed at the next apoapsis passage. One way in which to ensure this is to plan trajectories that do not have a significant decrease in orbit period following flyby of the asteroid. This is a real issue, as the orbit period can be cut significantly as a function of flyby conditions, placing the spacecraft into an orbit with a relatively low apoapsis and subjecting the spacecraft to a strong gravitational perturbation. The effect of this on the uncertain spacecraft trajectory can lead to a significant degradation of state information and could place the spacecraft into an impacting or escaping orbit. Conversely, if the flyby is designed to increase the orbit period, and hence the orbit apoapsis, there is an added degree of robustness for the spacecraft. Using the results of the previous section, we can develop an explicit design approach to choosing the flyby conditions appropriately.

First, we can note that the integral I_2^1 dominates the expression for change in orbit energy over a full pass. Thus, we know that the change in energy (and angular momentum) that an orbit receives during a close flyby will be proportional to

$$\Delta C \;\propto\; -\cos^4\frac{i}{2}\sin 2(\Omega+\omega) \tag{34}$$

where Ω is the longitude of the ascending node in the body-fixed frame at periapsis and ω is the argument of periapsis in the body-fixed frame at periapsis. Thus, to maximize the increase in energy for a particular flyover, we must choose $\tilde{\omega} = \Omega + \omega$ to maximize $-\sin 2\tilde{\omega}$. If we wish to constrain energy so that it does not decrease, then choose $\tilde{\omega}$ such that $-\sin 2\tilde{\omega} > 0$.

Simple analysis shows that the maximum increase of energy occurs when

$$\tilde{\omega} = (2m+1)\frac{\pi}{2} \tag{35}$$

and that an increase in energy will occur whenever

$$(2m-1)\frac{\pi}{2} < \tilde{\omega} < m\pi \tag{36}$$

It is, of course, possible to further restrict the intervals of $\tilde{\omega}$ in order to ensure a change of energy within a particular range. This then presents us with our target values of $\tilde{\omega}$ in order to ensure the desired flyby result.

Now, prior to the low-altitude flyover, we assume that the spacecraft is in a circular orbit at a safe altitude and with its orbit plane at a particular inclination with respect to the asteroid equator. Assuming that a nominal low-altitude flyover ellipse has been chosen, the main design issue will be the timing of the initial de-orbit maneuver. Once this maneuver occurs, the spacecraft trajectory is set.

We assume that at an initial epoch the spacecraft ascends through the equatorial plane at a body-fixed longitude of λ_o. Then at any time t after the initial epoch, the longitude of the ascending node in the body-fixed frame is computed as

$$\Omega = \lambda_o + \dot{\Omega}_{J_2} t - \omega_E t \tag{37}$$

where $\dot{\Omega}_{J_2}$ is the node precession rate and ω_E is the Eros rotation rate. In general, $|\omega_E| \gg |\dot{\Omega}_{J_2}|$. While in the circular orbit, the spacecraft can de-orbit into an elliptic transfer down to a low periapsis. For a given transfer orbit, the orbit period will be T_T. At periapsis the longitude of the ascending node in the body-fixed frame, given a de-orbit maneuver at time t, is then

$$\Omega = \lambda_o + \left(\dot{\Omega}_{J_2} - \omega_E\right)\left(t + \frac{T_T}{2}\right) \tag{38}$$

We can also measure the in-plane angle from the initial equatorial crossing in our circular orbit as

$$M = \bar{n} t \tag{39}$$

where $\bar{n}$ is the mean motion for the spacecraft orbit incorporating oblateness effects. Then given a de-orbit maneuver at time t, the argument of periapsis of the orbit at periapsis passage will be

$$\omega = \bar{n} t + \dot{\omega}_{J_2} \frac{T_T}{2} + \pi \tag{40}$$

where $\dot{\omega}_{J_2}$ is the secular rate of the argument of periapsis due to the asteroid oblateness.

Thus, the combined expression for $\Omega + \omega = \tilde{\omega}$ is

$$\tilde{\omega} = \pi + \lambda_o + \dot{\tilde{\omega}}_{J_2} \frac{T_T}{2} - \left(\dot{\theta} - \bar{n} - \dot{\Omega}_{J_2}\right) t \tag{41}$$

Whenever this expression is equal to $(4m-1)\pi/4$, a maneuver will send the spacecraft onto a trajectory that gives it the largest energy kick, and whenever it lies in the interval $[(2m-1)\pi/2, m\pi]$, it will yield an increase in energy.

The period between two such encounters is

$$T_R = \frac{\pi}{\dot{\theta} - \bar{n} - \dot{\Omega}_{J_2}} \tag{42}$$

For a 50-km circular orbit, this is approximately 3.2 hours.

Given a specified maneuver time t, we use the above formulae to compute the body-fixed Ω and ω at the time of periapsis passage. This in turn maps into a periapsis vector location (latitude δ, longitude λ) in the Eros body-fixed frame:

$$\cos\delta\cos\lambda = \cos\omega\cos\Omega - \sin\omega\sin\Omega\cos i \tag{43}$$

$$\cos\delta\sin\lambda = \cos\omega\sin\Omega + \sin\omega\cos\Omega\cos i \tag{44}$$

$$\sin\delta = \sin\omega\sin i \tag{45}$$

Note the mapping $(\omega, \Omega) \rightarrow (\delta, \lambda)$ is not one-to-one. For every periapsis location in the body-fixed frame, there are in general two values of ω and Ω that will lead to the same location. Specifically, if $(\omega, \Omega) \rightarrow (\delta, \lambda)$, then $(\omega', \Omega') \rightarrow (\delta, \lambda)$, where

$$\omega' = \pi - \omega \tag{46}$$

$$\tan(\lambda - \Omega') = -\tan\omega\cos i \tag{47}$$

In Figs. 4 through 6, the traces of periapsis locations in the asteroid-fixed frame that provide a zero, positive, and negative change in energy are plotted by themselves, and with a sample trajectory to indicate the sequence of design opportunities.

It is instructive to look at the dynamics of a spacecraft trajectory after following such a low-altitude flyover. To that end a series of Monte Carlo runs was performed in support of the NEAR Shoemaker's October low-altitude flyover of the Eros surface. An example of a proposed flyover trajectory is given in Fig. 7, showing the radius of the trajectory as a function of time. According to the criteria proposed above, this trajectory is a good candidate for a series of low-altitude flyovers, as the apoapsis progressively increases, allowing for the possibility of a relaxed update schedule and small adjustments at each apoapsis passage. However, when looked at as the evolution of a statistical distribution of trajectories, we see that the proposed trajectory may not be safe to continue beyond its initial transition to apoapsis. Assuming relatively conservative state uncertainties of 10 m in position and 1 cm/s in velocity, 1000 trajectories were integrated over the three apoapsis passages shown in Fig. 7. In Figs. 8 through 10, histograms from these trajectories are shown at each of the apoapsis passages, showing the distribution of periapsis and apoapsis radii and the time deviation from the nominal apoapsis passage. Thus, we see that the trajectories are rapidly dispersed about the asteroid, indicating a strong possibility that the spacecraft trajectory knowledge could be substantially compromised and navigation of the craft made difficult unless special precautions are taken.

B. Landing Design

A landing trajectory is really a two-point boundary value problem, where the spacecraft must be carried from its initial trajectory to a desired location on the asteroid surface. Thus, design of a landing trajectory is most conveniently divided into two separate problems, one that goes forward in time and one that goes backwards in time, and to complete the design these two trajectories must be matched with each other at some midpoint.

The elements of the forward design are to constrain the initial trajectory and the timing of the initial transfer maneuvers. The forward design is most concerned with the initial de-orbit maneuver and ensuring that the asteroid is at the proper phase angle once the spacecraft has reached a low altitude relative to the asteroid. For a realistic design, at least one or two braking maneuvers should be incorporated to ensure that the overall timing of the transfer is consistent with the final, desired maneuver. Using approximate results, such as simple two-body orbit elements at the least or corrections to these using the analytic theory discussed in the article, the initial inertial location of the spacecraft at descent commencement can be found such that the spacecraft is close to the desired location on the asteroid surface at the end of the maneuver sequence.

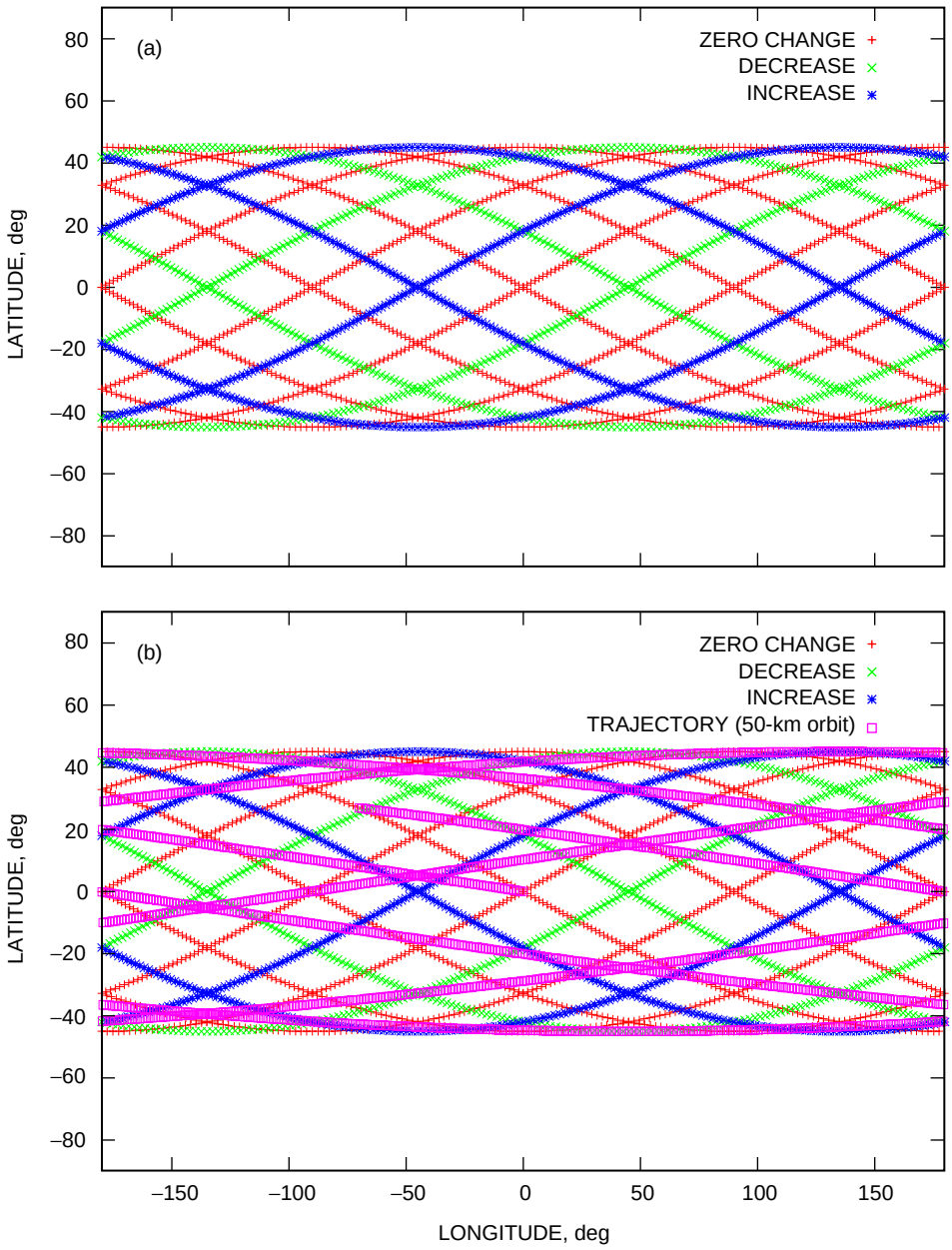

Fig. 4. Periapsis locations in the asteroid-fixed frame: (a) regions of energy increase, decrease, and zero change mapped onto the asteroid surface for an inclination of 135 deg and (b) the same as (a) with the trajectory of a spacecraft in a 50-km orbit with an inclination of 135 deg superimposed.

The backwards design is less conventional and starts from the desired landing state, location on the asteroid surface, and time. The desired landing velocity vector is assumed to be normal to the asteroid surface, and the resulting trajectory is found by integrating backwards in time (in the body-fixed coordinate system with a non-divergent gravity field description). Resulting from the first stage of this approach, the trajectory will reach apoapsis relatively soon (assuming a small impact speed) and will then descend back to the surface again. The last braking maneuver is designed close to this apoapsis and consists of a maneuver of fixed size and direction, chosen to boost the trajectory apoapsis to a higher altitude. This iteration is continued until the spacecraft is boosted to the first braking maneuver, which nominally takes the spacecraft trajectory from a transfer ellipse with periapsis above the asteroid surface

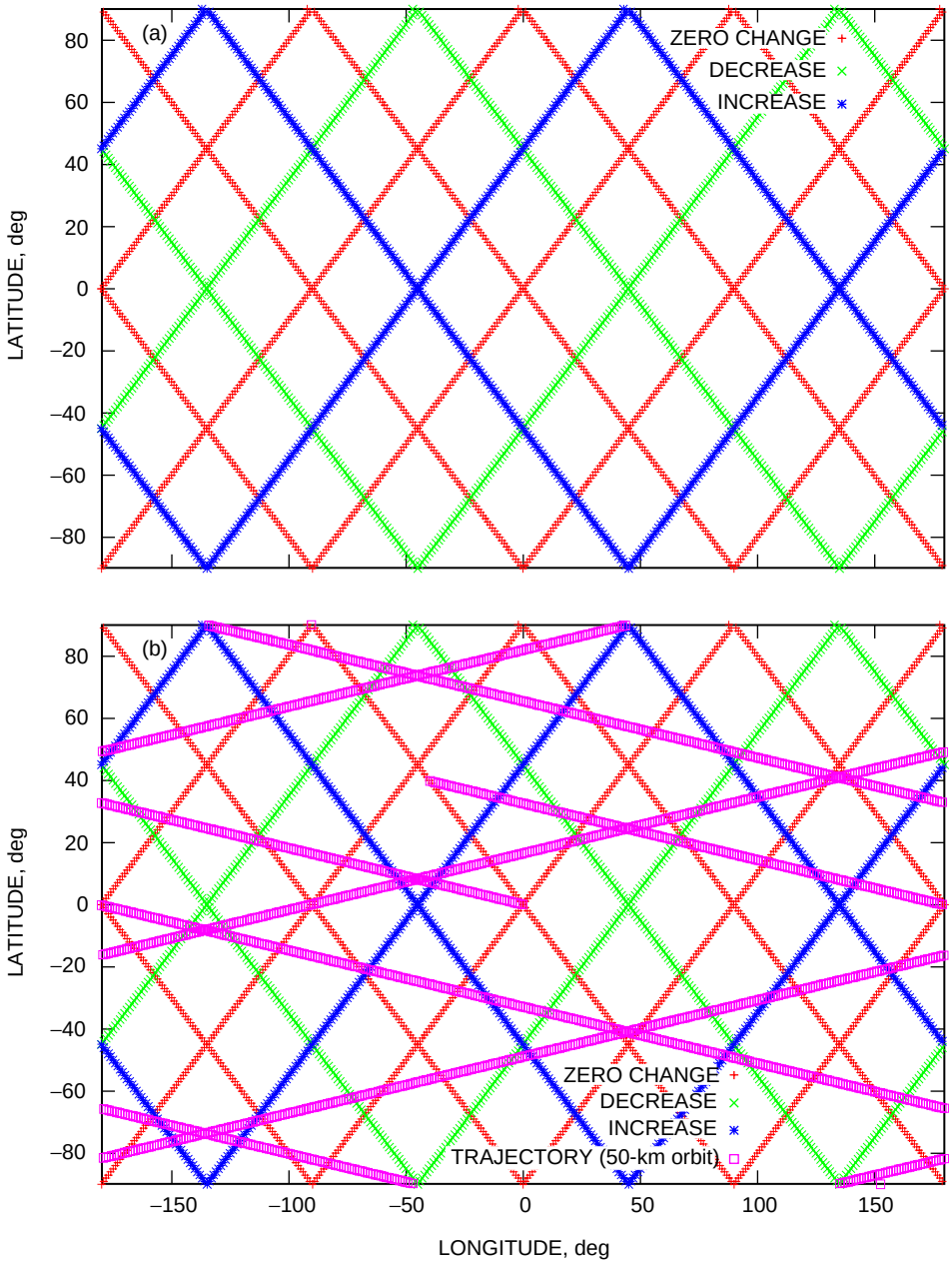

Fig. 5. Periapsis locations in the asteroid-fixed frame: (a) regions of energy increase, decrease, and zero change mapped onto the asteroid surface for an inclination of 90 deg and (b) the same as (a) with the trajectory of a spacecraft in a 50-km orbit with an inclination of 90 deg superimposed.

to an impact trajectory with periapsis deep within the asteroid. Based on the desired characteristics of the transfer ellipse, the size and magnitude of this maneuver are chosen to give the transfer ellipse the desired energy, angular momentum, and plane orientation. Nominally, the backwards integration can then take the trajectory all the way back to apoapsis, but in general there will be a disconnect between the desired starting point (found from the forward design sequence) and the resulting end point of the backwards integration.

To resolve the discontinuity, the forward and backward segments of the trajectory must be matched. The logical location for this match point is at the transition from the descent ellipse periapsis to the

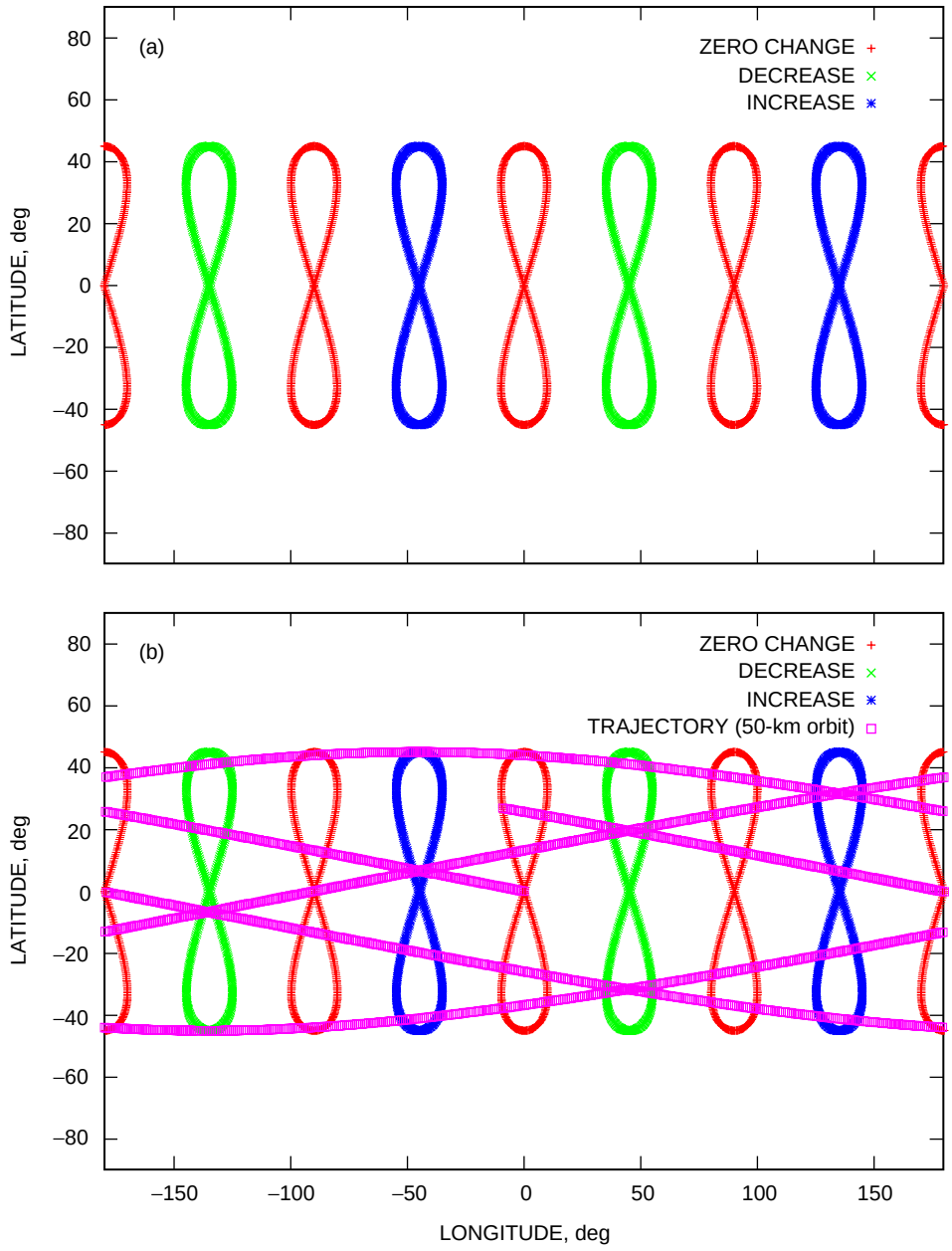

Fig. 6. Periapsis locations in the asteroid-fixed frame: (a) regions of energy increase, decrease, and zero change mapped onto the asteroid surface for an inclination of 45 deg and (b) the same as (a) with the trajectory of a spacecraft in a 50-km orbit with an inclination of 45 deg superimposed.

initial impact trajectory. After this point, the nominal trajectory should be on the precision-targeted trajectory in order to impact the surface with the appropriate state and hence should follow the backwards integration. Also, this maneuver will be large enough in general that it will be able to accommodate the additional ΔV needed to bring the elements into line. If the forward design "stand-in" descent maneuvers were not chosen realistically enough, it may be difficult to match the trajectories. In this case, the forward design should be modified appropriately and the entire process repeated. Note that the initial forward design is the most difficult and open-ended element of the process, and that the precision nominal trajectory during the descent phase can be generated almost automatically, once the appropriate tools have been created and the nominal landing site, conditions, and time have been chosen.

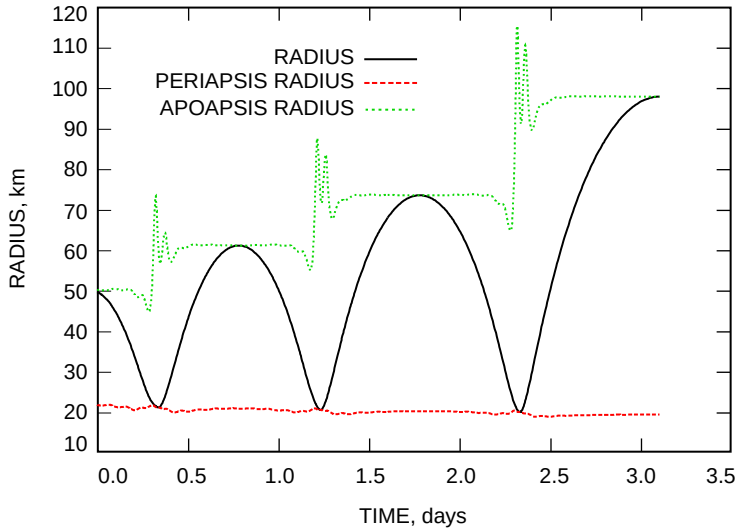

Fig. 7. The radius of a series of low-altitude flyovers taken in succession, taken from the nominal trajectory for which the Monte Carlo runs were performed.

V. Conclusion

This article gives a basic design methodology that can be used in the planning of low-altitude flyovers and landing trajectories for a spacecraft orbiting an asteroid or comet. Some analytical results that can be used for these design purposes are derived and described, and numerical simulations of some trajectories are presented.

References

[1] P. G. Antreasian, C. E. Helfrich, J. K. Miller, W. M. Owen, B. G. Williams, D. K. Yeomans, J. D. Giorgini, D. W. Dunham, R. W. Farquhar, J. V. McAdams, and D. J. Scheeres, "Preliminary Considerations for NEAR's Low-Altitude Passes and Landing Operations at 433 Eros," AIAA Paper 98-4397, presented at the 1998 Astrodynamics Specialist Meeting, Boston, Massachusetts, August 1998.

[2] D. Brouwer and G. M. Clemence, *Methods of Celestial Mechanics*, New York: Academic Press, 1961.

[3] B. Chauvineau, P. Farinella, and F. Mignard, "Planar Orbits about a Triaxial Body: Application to Asteroidal Satellites," *Icarus*, vol. 105, pp. 370–384, 1993.

[4] J. K. Miller, W. E. Bollman, R. P. Davis, C. E. Helfrich, D. J. Scheeres, S. P. Synnott, T. C. Wang, B. Williams, and D. K. Yeomans, "Navigation Analysis for Eros Rendezvous and Orbital Phases," *Journal of the Astronautical Sciences*, vol. 43, pp. 453–476, 1995.

[5] S. Sawai and D. J. Scheeres. "Control of Hovering Spacecraft Using Altimetry," AIAA Paper 2000-4421, presented at the 2000 AIAA/AAS Astrodynamics Specialist Meeting, Denver, Colorado, August 2000.

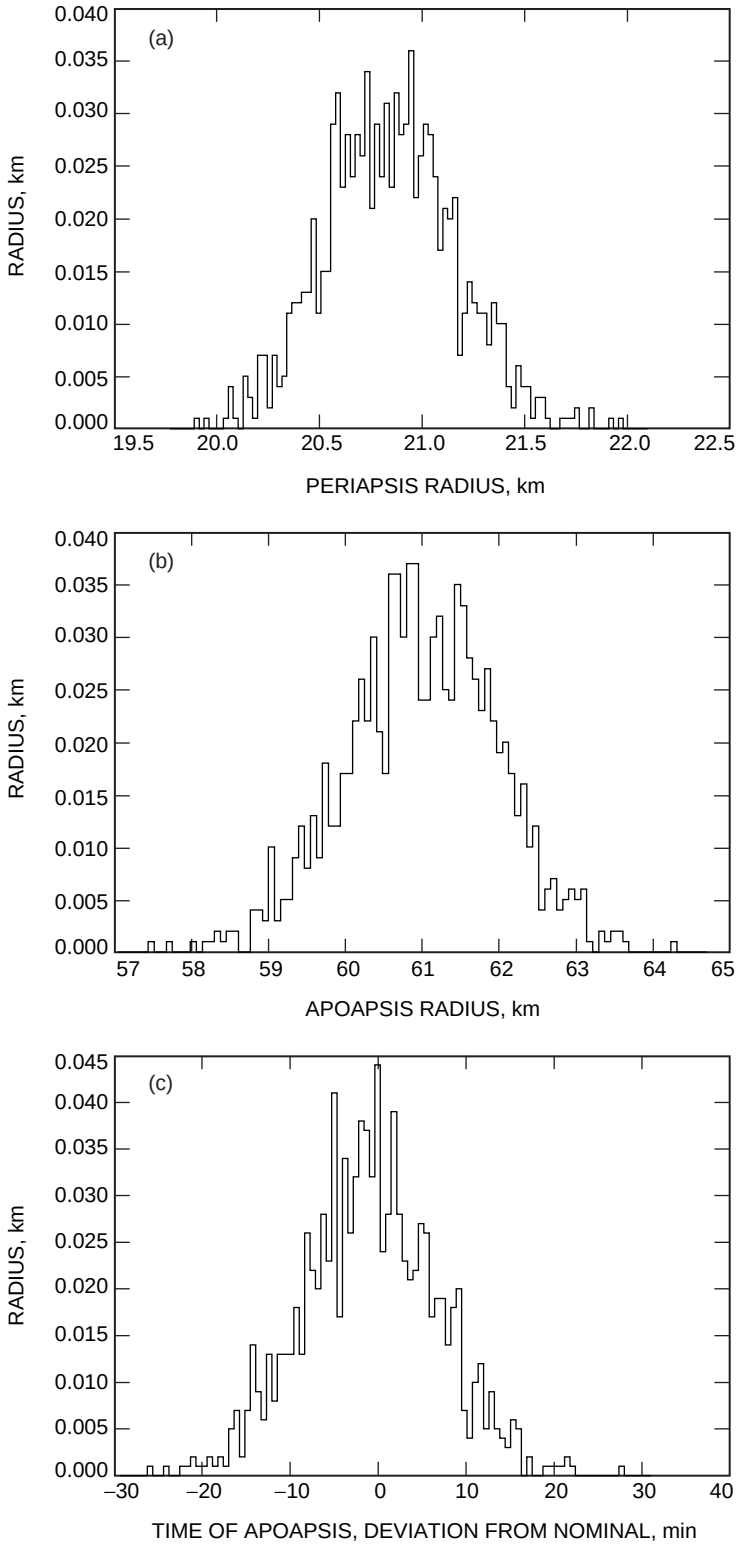

Fig. 8. Histograms taken at the first apoapsis passage: (a) periapsis radii, (b) apoapsis radii, and (c) time deviation from the nominal apoapsis passage.

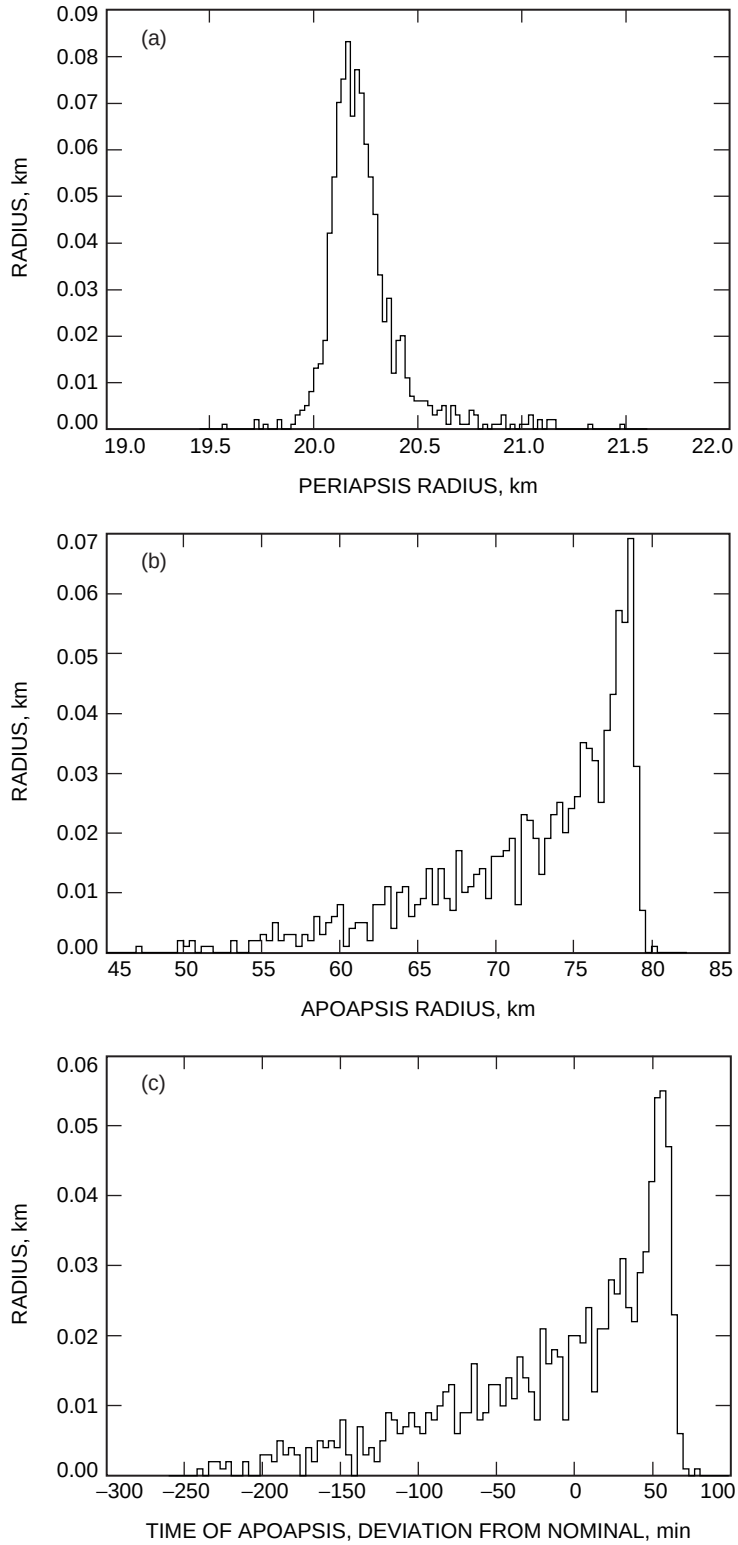

Fig. 9. Histograms taken at the second apoapsis passage: (a) periapsis radii, (b) apoapsis radii, and (c) time deviation from the nominal apoapsis passage.

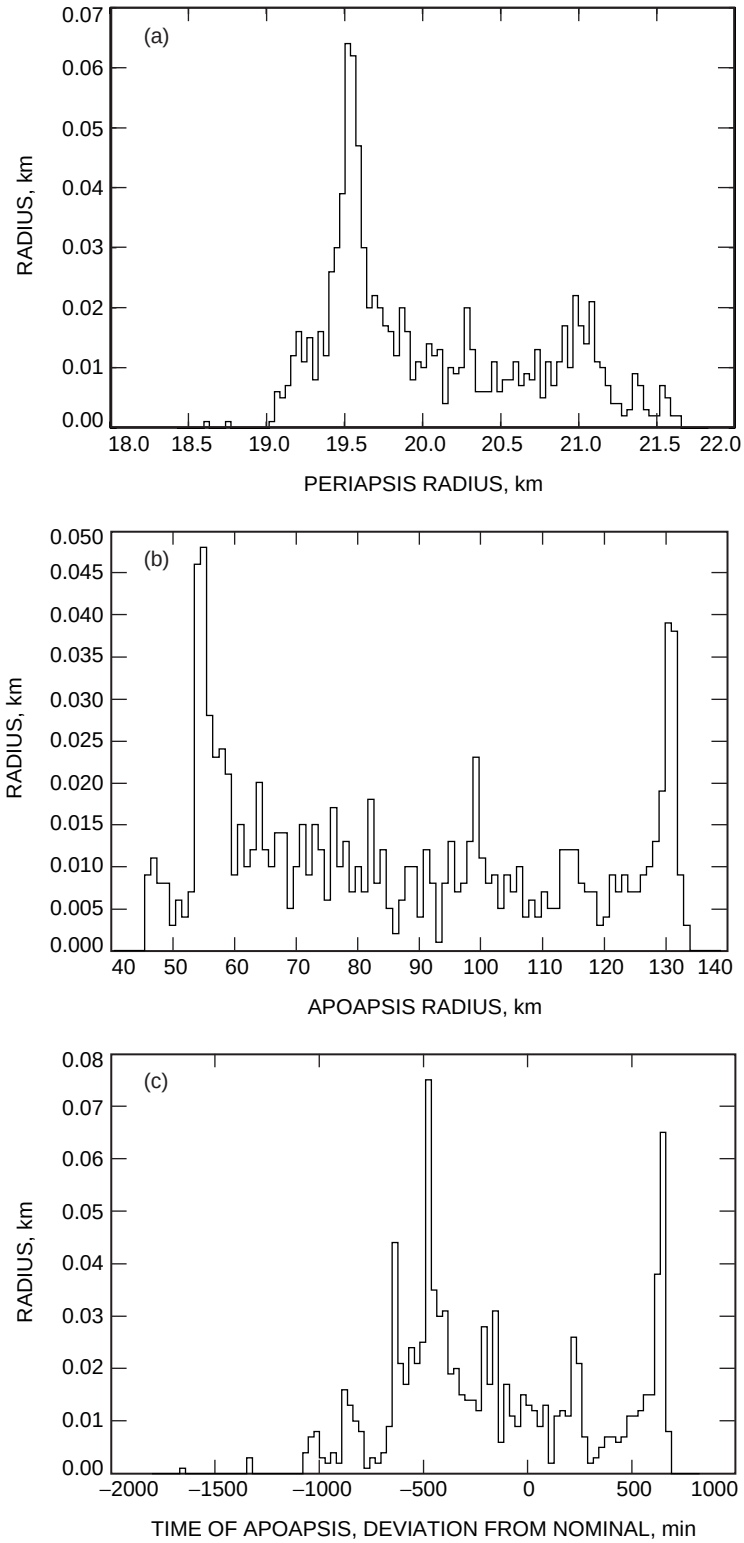

Fig. 10. Histograms taken at the third apoapsis passage: (a) periapsis radii, (b) apoapsis radii, and (c) time deviation from the nominal apoapsis passage.

[6] D. J. Scheeres, "Dynamics about Uniformly Rotating TriAxial Ellipsoids: Applications to Asteroids," *Icarus*, vol. 110, pp. 225–238, 1994.

[7] D. J. Scheeres, "Analysis of Orbital Motion Around 433 Eros," *Journal of the Astronautical Sciences*, vol. 43, pp. 427–452, 1995.

[8] D. J. Scheeres, S. J. Ostro, R. S. Hudson, and R. A. Werner, "Orbits Close to Asteroid 4769 Castalia," *Icarus*, vol. 121, pp. 67–87, 1996.

[9] D. J. Scheeres, "The Effect of C_{22} on Orbit Energy and Angular Momentum," *Celestial Mechanics and Dynamical Astronomy*, vol. 73, pp. 339–348, 1999.

[10] D. J. Scheeres, "Stability of Hovering Orbits Around Small Bodies," AAS Paper 99-159, presented at the 1999 AAS/AIAA Spaceflight Mechanics Meeting, Breckenridge, Colorado, February 1999.

[11] D. J. Scheeres, B. G. Williams, and J. K. Miller, "Evaluation of the Dynamic Environment of an Asteroid: Applications to 433 Eros," *Journal of Guidance, Control, and Dynamics*, vol. 23, no. 3, pp. 466–475, 2000.

[12] D. J. Scheeres, "Changes in Rotational Angular Momentum due to Gravitational Interactions between Two Finite Bodies," *Celestial Mechanics and Dynamical Astronomy*, in press.

[13] B. Villac, D. J. Scheeres, L. A. D'Amario, and M. D. Guman, "The Effect of Tidal Forces on Orbit Transfers," AAS Paper 01-247, presented at the 2001 AAS/AIAA Spaceflight Mechanics Meeting, Santa Barbara, California, February 2001.

[14] R. A. Werner and D. J. Scheeres, "Exterior Gravitation of a Polyhedron Derived and Compared with Harmonic and Mascon Gravitation Representations of Asteroid 4769 Castalia," *Celestial Mechanics and Dynamical Astronomy*, vol. 65, pp. 313–344, 1997.

[15] R. A. Werner, "The Gravitational Potential of a Homogeneous Polyhedron," *Celestial Mechanics and Dynamical Astronomy*, vol. 59, pp. 253–278, 1994.